PERGAMON

Journal of Structural Geology 25 (2003) 1901–1915

JOURNAL OF STRUCTURAL GEOLOGY

www.elsevier.com/locate/jsg

Characteristics and dynamic origin of the large-scale Jiaoluotage ductile compressional zone in the eastern Tianshan Mountains, China

Xing-Wang Xu[a,*], Tian-Lin Ma[b], Li-Qian Sun[b], Xin-Ping Cai[a]

[a]*Institute of Geology and Geophysics, CAS, PO Box 9825, Beijing 100029, China*
[b]*Institute of Geomechanics, CAGS, Beijing 100081, China*

Received 17 July 2001; received in revised form 10 December 2002; accepted 22 January 2003

Abstract

The Jiaoluotage ductile compressional zone (JDCZ) in the eastern Tianshan Mountains, China, developed in volcanic and sedimentary rocks that were deposited in a Carboniferous back-arc basin situated between the Jungar plate and middle Tianshan terrane. The ductile compressional zone, ~500 km long and 20–50 km wide, consists of a number of east-trending vertical foliation zones that display an augen geometry in plan view and a fan-like geometry in transverse profiles. Ductile compressional deformation has produced pervasive foliation, radial stretching lineations, contemporaneous folds, and various macroscopic to microscopic symmetric structures within the JDCZ. Rotations of most clasts and porphyroclasts are bidirectional. The preferred orientation patterns of the optical axes of calcite and quartz display axial or orthorhombic symmetry. Three kinds of strain patterns have been determined in the JDCZ: apparent flattening, plane strain and apparent constriction. The overall strain character of the JDCZ is 'cream-cake' style. The volcanic and sedimentary rocks within the JDCZ were metamorphosed into greenschist facies with temperature of 400–600 °C and pressure of 300–400 MPa. Development of the JDCZ is interpreted as due to N–S coaxial compression caused by the collision between the Tarim plate and the middle Tianshan arc–Jiaoluotage basin–Jungar plate system during the Permian between 270 and 290 Ma.

Keywords: Symmetric fabrics; Radial lineation; 'Cream-cake' strain style; Eastern Tianshan Mountains

1. Introduction

Since Clough (1897) put forward the concept of ductile faulting and Griggs (1936, 1940) carried out his famous experiments, ductile deformation has been considered as an important tectonic mechanism (Lee, 1945, 1946; Wang, 1949). Since the 1970s, the concept of ductile shear zones (Ramsay and Graham 1970) has been advanced significantly (e.g. Ramsay, 1980; White et al., 1980; Zheng and Chang, 1985; Ramsay and Huber, 1987; Zheng et al., 1988).

Recent studies suggest that high strain zones are not confined to a simple shear and plain-strain model, and ductile deformation zones with apparent flattening and constriction have also been reported (e.g. Choukroune and Gapais, 1983; Fletcher and Bartley, 1994; Bauer and Hudleston, 1995). Sanderson and Marchini (1984) used the term 'transpression' to refer to three-dimensional high-strain zones that were caused by oblique convergence and characterized by horizontal shortening and vertical lengthening.

Ramsay and Huber (1987) suggested that some high-strain zones with a 'cream cake' strain pattern may be induced by coaxial compression and they are referred to as ductile compressional zone (DCZ) by Yue and Ma (1990). This paper describes the large-scale Jiaoluotage ductile compressional zone (JDCZ) with symmetric fabrics and a 'cream-cake' strain character in the eastern Tianshan Mountains, China.

2. Geological setting

The JDCZ situated to the south of the Tuha basin is a part of the Jiaoluotage tectonic belt in the eastern Tianshan Mountains (Fig. 1a). The tectonic belt, composed of Carboniferous volcanic and sedimentary rocks, is located between the middle Tianshan terrane and Jungar plate.

* Corresponding author. Tel.: +86-10-62007331; fax: +86-10-62010846.
E-mail address: xuxw@mail.igcas.ac.cn (X.W. Xu).

0191-8141/03/$ - see front matter © 2003 Elsevier Ltd. All rights reserved.
doi:10.1016/S0191-8141(03)00017-8

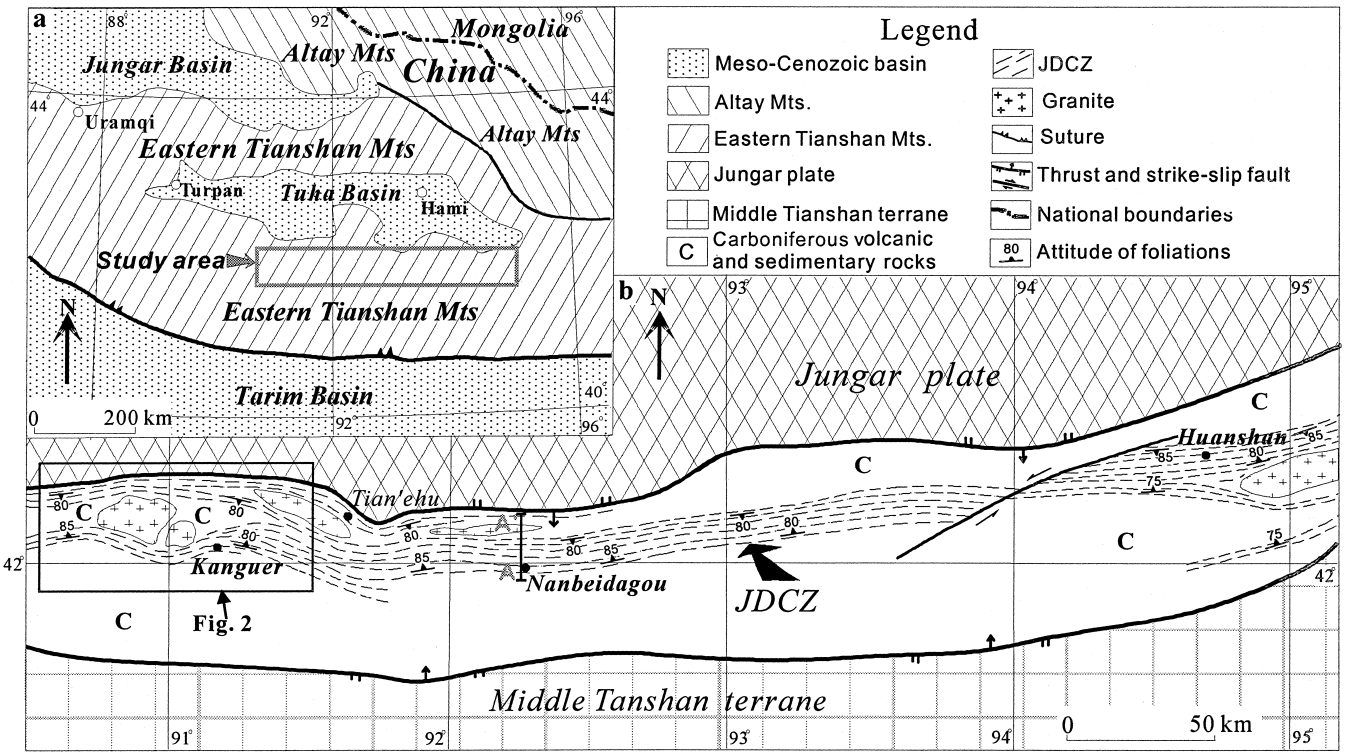

Fig. 1. Tectonic setting (a) and distribution (b) of the JDCZ. Line A–A′ shows location of profile A–A′ in Fig. 3.

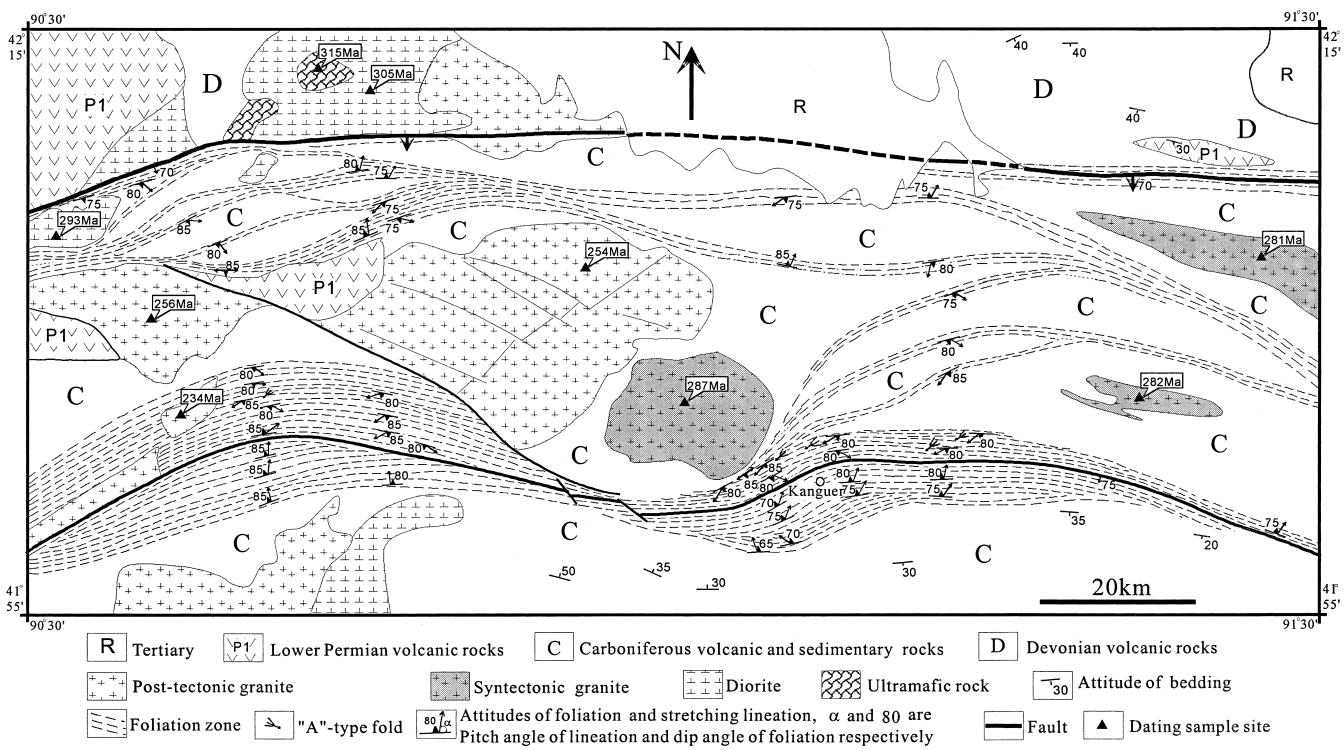

Fig. 2. Distribution of vertical foliation zones within the JDCZ in the Kanguer area. The location of this illustration is shown in Fig. 1. Intrusive ages after Ji et al. (1994), Hu et al. (1997) and Yang et al. (1999).

The Carboniferous volcanic and sedimentary rocks within the Jiaoluotage tectonic belt are divided into the Yamengshu and Ganduan Formations. The Yamengshu Formation (C_{1y}) consists of basalt and sandstone in the lower part, andesite and andesitic pyroclastic rocks in the middle part, and limestone and fine-grained clastic sedimentary rocks in the upper part. The 5000-m-thick Yamengshu Formation is mainly present in the northern and southern parts of the volcano-sedimentary basin. The 3000-m-thick Ganduan Formation (C_{2g}) consists of sandstone, conglomerate, limestone, bioclastic limestone, pelite, and siliceous rocks. It is mainly present in the middle part of the volcano-sedimentary basin. The basin was a back-arc basin related to the northward subduction of the Tarim Paleo-ocean plate under the Jungar plate (Ma et al., 1990; Xiao and Feng, 1990). The Carboniferous volcanic and sedimentary rocks underwent greenschist facies metamorphism from 276 ± 7 to 290 ± 7 Ma (Rb–Sr and Sm–Nd ages; Yang et al., 1999).

There are abundant Hercynian intrusive rocks in the Jiaoluotage tectonic belt that include ultramafic rocks, diorite, and granites. The ultramafic rocks and diorites were intruded between 296 and 316 Ma, after the first deformation event (Hu et al., 1997). Some syntectonic granites of dripshape or irregular bands intruded into weakly deformed blocks within the JDCZ between 260 and 287 Ma (Ji et al., 1994; Yang et al., 1999). Other granites intruded after the formation of the JDCZ, with ages ranging from 210 to 250 Ma (Ji et al., 1994).

The Jiaoluotage tectonic belt contains four generations of E–W-trending structures: D_1 folds, D_2 vertical foliation zones, D_3 conjugate low-angle brittle fractures, and D_4 strike-slip faults. The D_1 folds are broad and gentle. Folded bedding is overprinted and strongly transposed by an S_2 vertical foliation. The S_2 vertical foliation is truncated by the D_3 conjugate low-angle brittle fractures and by D_4 strike-slip faults. The vertical foliation zone with symmetric fabrics developed during the main compressional tectonic event (D_2) is referred to as the JDCZ. They are unconformably overlain by Permian conglomerates and sandstones.

3. Geometry of the JDCZ

The E–W-trending JDCZ is distributed in an area between 90°30′ and 95°30′E longitude, 42° and 42°30′N latitude (Fig. 1b). It is more than 500 km long, and 20–50 km wide. It consists of several vertical foliation zones that have different geometries in different parts.

In the western part (Kanguer area; Fig. 2) of the JDCZ, anastomosing foliation zones form a phacoidal geometry. Several augen structures are present in the northern arcuate foliation zone, and from west to east their strikes change from SW to W to NW. In the eastern part of Fig. 2, foliations converge towards a point south of syntectonic granite. In the southwestern part of Fig. 2, an arcuate foliation zone is convex northwards. Diorite and syntectonic granite are common in weakly deformed symmetrical phacoids.

The E–W-trending foliations in the Nanbeidagou area in the middle part of the JDCZ are distributed in parallel strips in plan view and have a symmetrical fan-shape in cross-section (Fig. 3). In the eastern part of the JDCZ (Fig. 1), the vertical foliation zones in the Huanshan area have a symmetrical lozenge shape that trend E–W.

4. Ductile deformation features

4.1. Foliation and stretching lineations

Foliation and stretching lineations in the JDCZ are defined by preferred alignment of metamorphic mica and crystallized calcite and quartz. The foliation (Fig. 4a and b) is parallel to the boundaries of its host deformation zone and generally dips 65–80° to the north or south. It is more pervasive in the central part of the JDCZ than the northern and southern outer zones.

Stretching lineations do not display a universal orientation throughout the JDCZ. Projections of stretching lineations from 188 sites that plunge 0–90° to either the east or west are distributed in an E–W great circle zone (Fig. 5). However, stretching lineations have a consistent orientation at outcrop-scale (Fig. 4c and d).

The attitudes of stretching lineations vary gradually along the strike of a foliation subzone from horizontal to downdip several times, forming several radial-style fans. For example in the Kanguer area (Fig. 2), the pitch angles of stretching lineations in the southeastern foliation zones vary from 0 to 50° from the convergent point to the east; the pitch angles of stretching lineations in the northern part of the southwestern arcuate foliation zone gradually change from 30°E, 30°W to 30–50°E, and they finally pitch to the west. The convergent points of stretching lineations are interpreted as the sites of intense shorting along the foliation subzones.

The attitudes of stretching lineations vary abruptly across adjacent foliation subzones, which indicates that these foliation subzones have deformed independently. Four major convergent points of radial-style stretching lineations

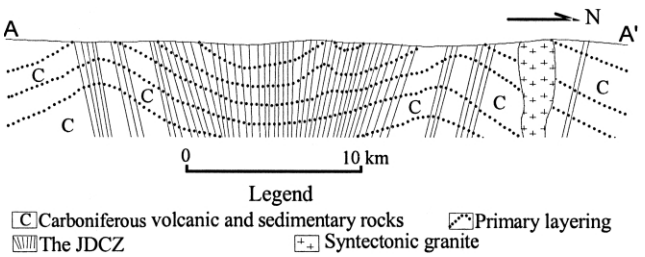

Fig. 3. A structural transverse profile (A–A′) in the Nanbeidagou area (see Fig. 1 for location).

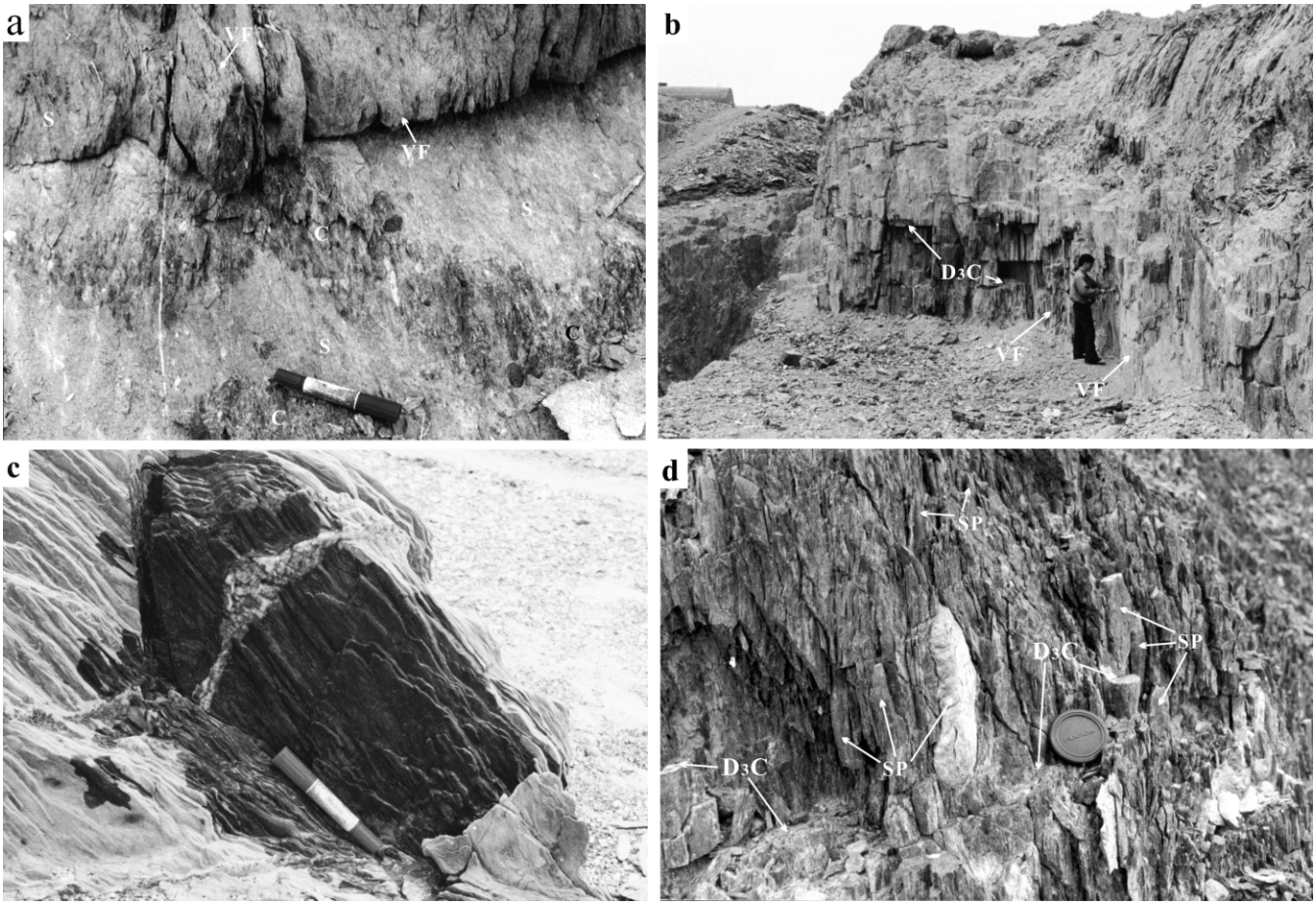

Fig. 4. Photographs show foliation and stretching lineation structures. (a) Folded conglomerates (C) and sandstone (S) were overprinted by *S*2 vertical foliations (VF) in the Huanshan area. The marker pen is 14 cm long. (b) *S*2 vertical foliations parallel to each other and to its host deformation zone, and cut by *D*3 lower-angle brittle fractures (D_3C) in the Kanguer area. The man is 162 cm high. (c) Stretching lineations on the vertical foliation surface in the Kanguer area. The marker pen is 14 cm long. (d) Stretched pebbles (SP) aligned parallel to the stretching lineations and cut by D_3 lower-angle brittle cleavages (D_3C) in the Huanshan area. The lens is 6 cm in diameter.

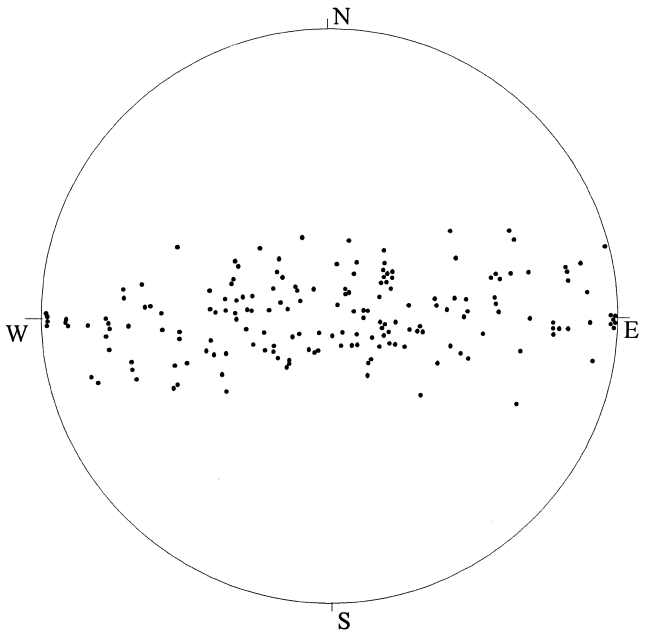

Fig. 5. Upper hemisphere, equal-area projections of stretching lineations from 188 sites in the JDCZ.

have been recognized in the Kanguer, Tian'ehu, Nanbeidagou, and Huanshan areas within the JDCZ (Fig. 6). Large syntectonic granites are intruded near the convergent points.

4.2. Contemporaneous folds and boudins

Contemporaneous folds (Williams, 1978) of foliations and boudin structures are developed at both macro- and micro-scales in intense deformation zones of the JDCZ. Most contemporaneous folds are 'A'-type folds, which can be divided into two subtypes: Z-asymmetric folds and symmetric upright folds (Fig. 7a). Symmetric upright folds may gradually evolve into Z-asymmetric folds (Fig. 7b). This suggests that the 'A'-type folds in the JDCZ may have resulted from localized shortening caused by flow-parallel perturbations (Holdsworth, 1990), rather than by hinge rotation (Sanderson, 1973; Bell, 1978; Williams, 1978).

Most boudin structures, including rectangular boudins (Fig. 7c) and thin lenticular boudins (Fig. 7d), are symmetric and parallel to the foliation zone with stretching axes parallel to the stretching lineations. Most rectangular

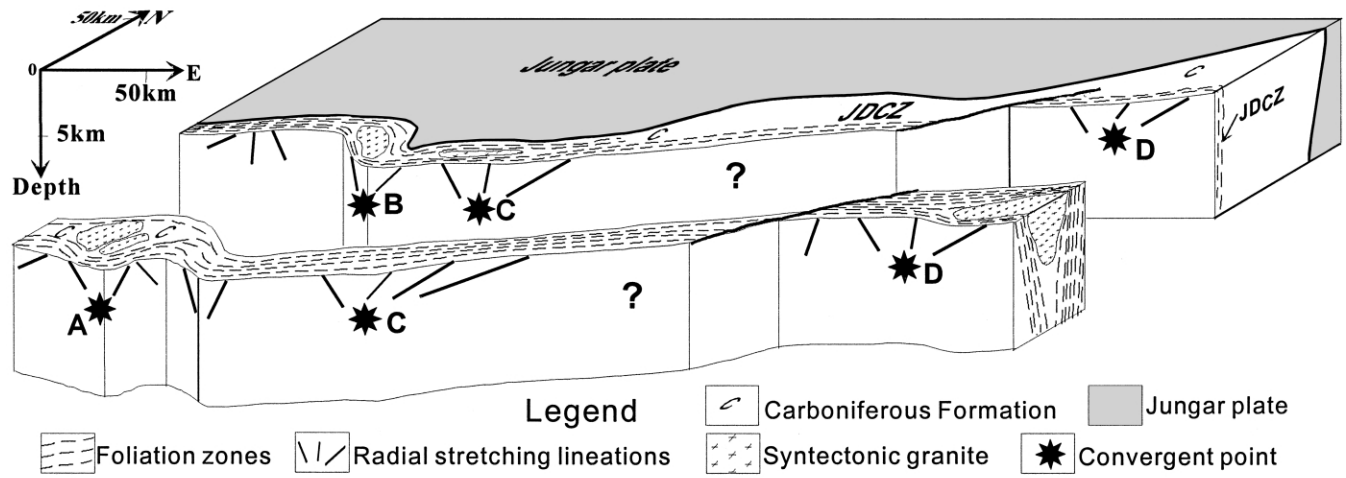

Fig. 6. Sketch showing stretching lineations and four convergent points in the JDCZ. Convergent points: (A) the Kangu'er area, (B) the Tian'ehu area, (C) the Nanbeidagou area and (D) the Huangshan area.

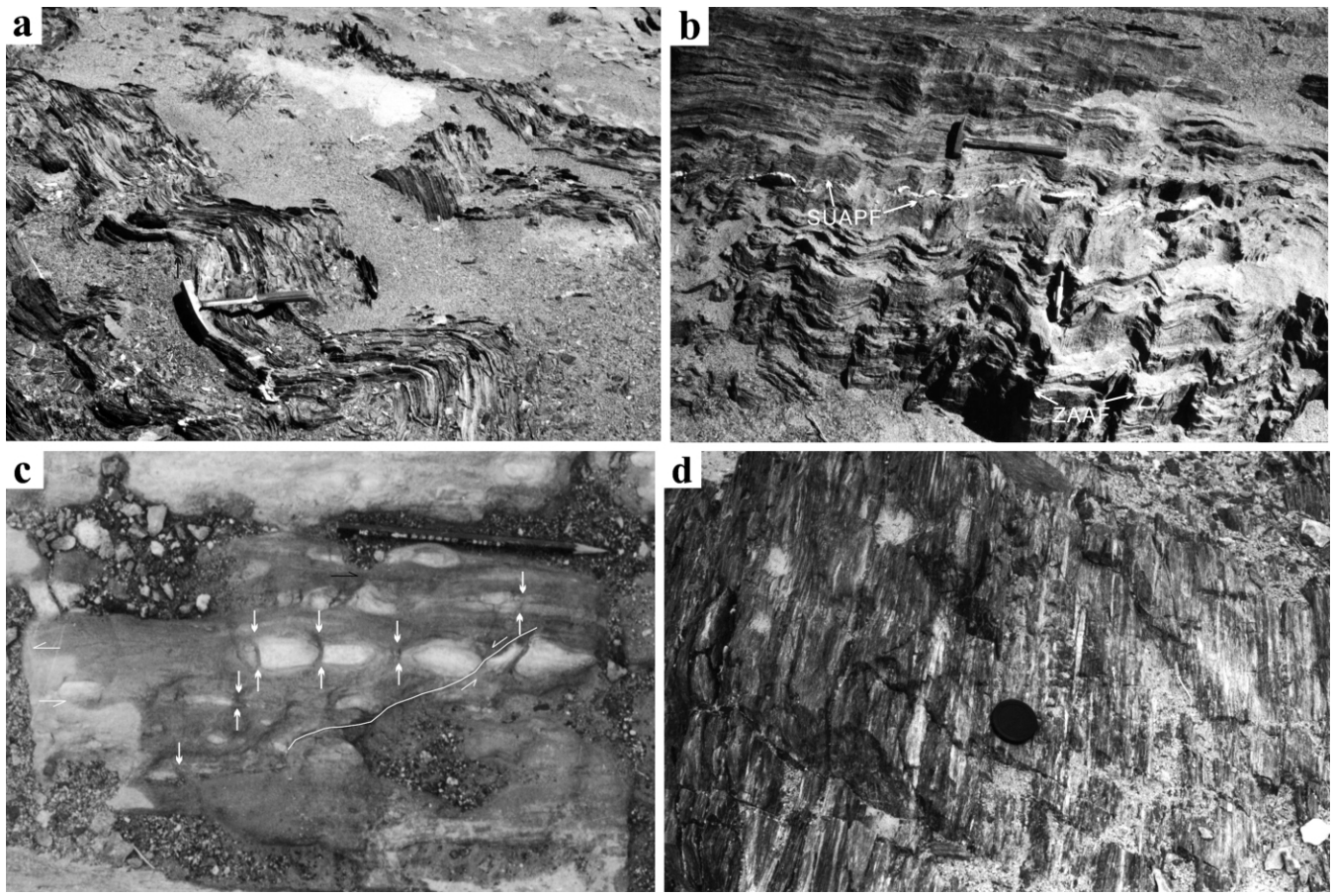

Fig. 7. Photographs show contemporaneous folds and boudin structures. (a) Wavy symmetric upright 'A'-type folds in the Huanshan area. The hammer is 30 cm long. (b) 'A'-type symmetric upright folds (SUF) and slightly Z-asymmetric 'A'-type folds (ZAAF) in the Huanshan area. The hammer is 30 cm long. (c) Rectangular boudins in the Nanbeidagou area. The pencil is 16 cm long. Arrows show shorting directions. (d) Thin lenticular boudins in the Huanshan area. The lens cover is 6 cm in diameter.

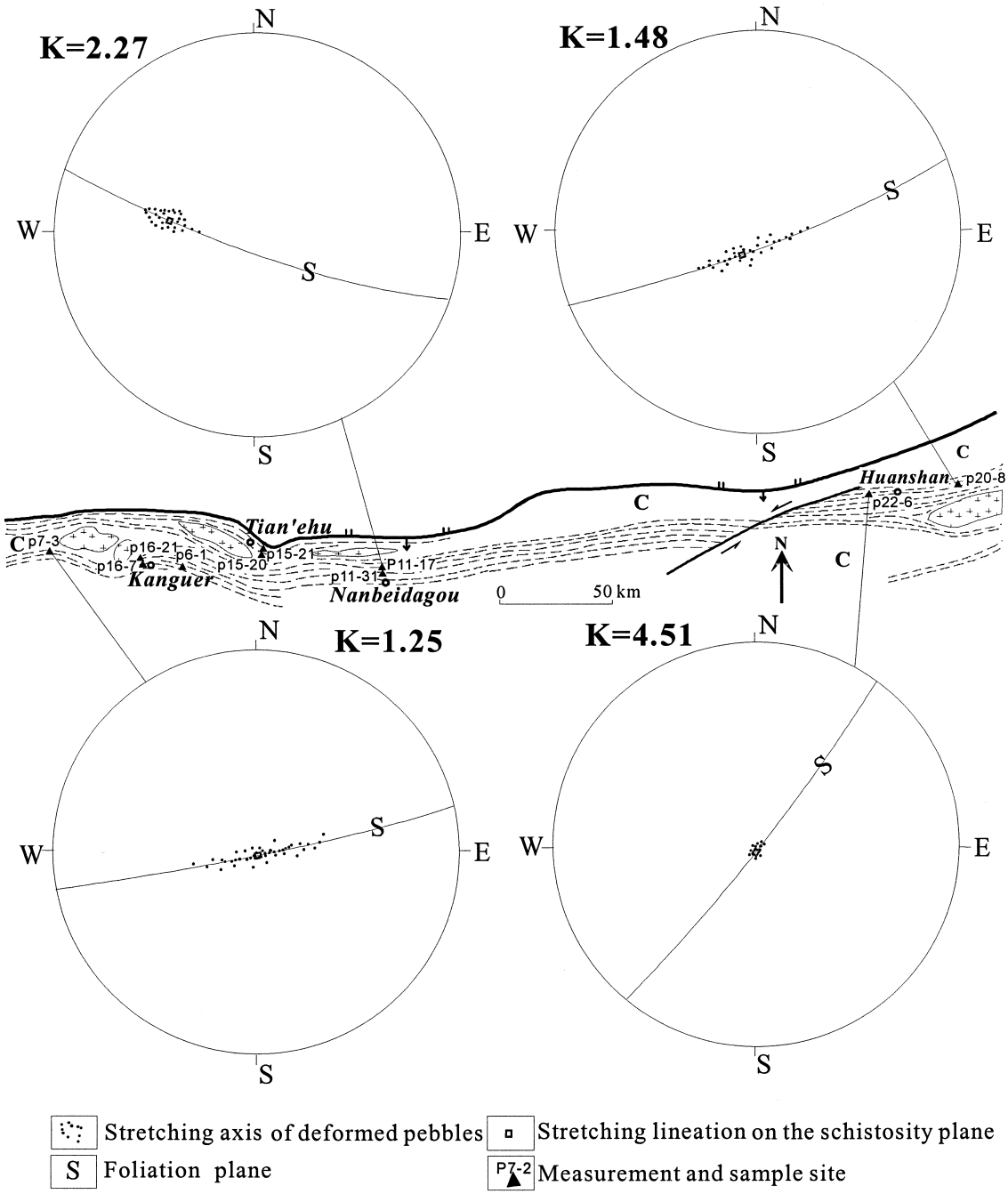

Fig. 8. Relationship among the attitudes of foliation, stretching lineations and deformed pebbles. Upper hemisphere and equal area projections. k represents Flinn *k* parameter. The sample sites of Figs. 10 and 11 are also shown.

boudins are present in the outer zones of the JDCZ, while thin lenticular boudins are most prevalent in the middle part of the intensive deformation zone.

4.3. Deformation of pebbles, clasts and porphyroclasts

Deformed pebbles, clasts and pyroclasts directly indicate the kinematic characters and deformation style of the JDCZ. Long axes of deformed pebbles are parallel to the foliations and stretching linations (Fig. 4d). Relations among the attitudes of foliations, stretching lineations and deformed pebbles, and their corresponding Flinn *k* parameter (Fig. 8) indicate that deformed pebbles are first rotated into parallelism with the foliations and then with the stretching lineations as stretching deformation proceeded progressively with increasing *k* value. Shapes of deformed pebbles are related to degree of deformation and strain pattern. Oblate ellipsoidal pebbles (Fig. 9a and b) are common in the outer subzones with an apparent flattening or a plane strain pattern, whereas elongated spindle and pencil-like pebbles

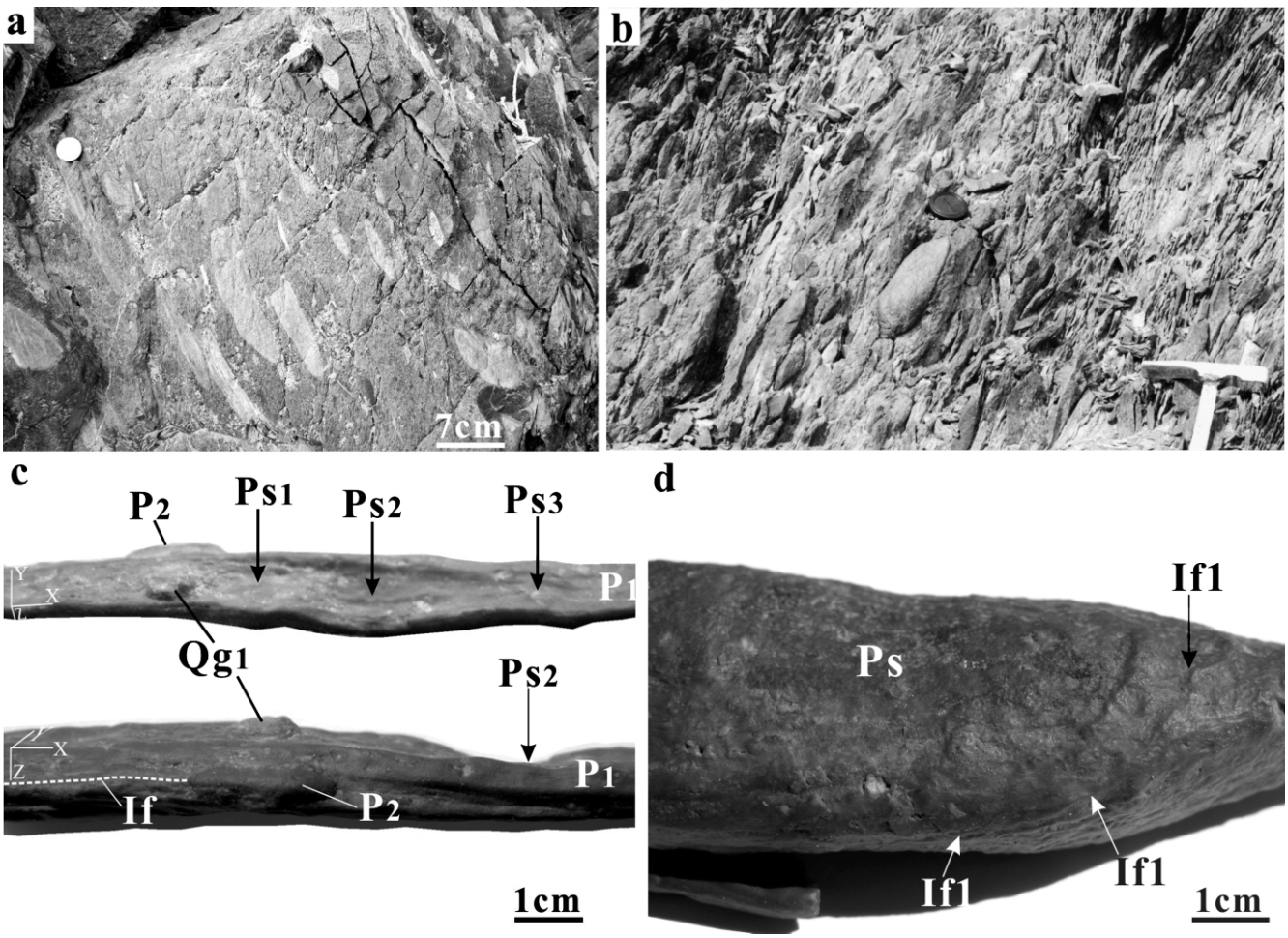

Fig. 9. Photographs show deformed pebbles. (a) Cake-like deformed pebbles in the Huanshan area. (b) Oblate ellipsoidal deformed pebbles in the Huanshan area. The lens cover is 6 cm in diameter. (c) Pit structures (e.g. Ps1, Ps2 and Ps3) are present on an oblate surface (*XY* plane) of a stretched pebble (P1), a quartz grain (Qg1) and a smaller stretched pebble are pitted into the P1 pebble. The intragranular foliation (If) of P1 deformed pebble is parallel to the elongation of their host pebble and adjacent pebble (P2). (d) A bigger pit structure (Ps) is associated by folded intragranular foliation in a deformed pebble.

(Fig. 4d) are well developed in the intensely deformed middle subzone. Pit structures are well developed on the deformed pebbles surfaces, especially on those surfaces parallel to the *XY* plane (Fig. 9c), suggesting intensive interaction between matrix and pebbles. Intragranular foliation within deformed pebbles is parallel to the elongation of the host pebble and the foliation in matrix generally (Fig. 9c), and thinned and folded beneath some bigger pitted structures (Fig. 9d). Bidirectional rotation of matrix grains (e.g. quartz and feldspar), folding of matrix grains and foliation in matrix (for example Q5 and Fz1 in Fig. 10), and symmetric necking and pitted structures (Fig. 10) indicate that ductile deformation of the conglomerates is due to a coaxial shortening perpendicular to the foliation (Fig. 10). Intensive stretching deformation of the pebbles in the JDCZ may be related to compression and pitting from adjacent smaller pebbles and matrix grains.

Deformation features of clasts are related to the lithology and deformation intensity of their host rocks. Clasts in pelitic and sandy schist are elongated parallel to the foliation (Fig. 11a) and their stretching axes are parallel to the stretching lineations. Symmetric pinch-and-swell structures suggest that these clasts were shortened perpendicular to the foliation. Pressure shadows in weakly deformed pyroclastic rocks are generally symmetric and aligned along the foliation (Fig. 11b).

Deformation in the pyroclastic rocks is weak. Rotation sense of feldspar and quartz pyroclasts is bidirectional. Intragranular conjugate fractures (Fig. 11c) and boudin structures were formed in quartz grains in the intensive deformational zones. These structures indicate coaxial shortening, although asymmetric boudins may have been induced by a local component of simple shear.

Porphyroclasts in mylonite and mylonitic schist derived from diorite and ultramatic rocks are lenticular and symmetric, but some asymmetric porphyroclasts show bidirectional shear senses. Occurrences of porphyroclasts with opposite shear senses in the same flowing zone (Fig. 11d) suggest that the relative movements are local and bidirectional.

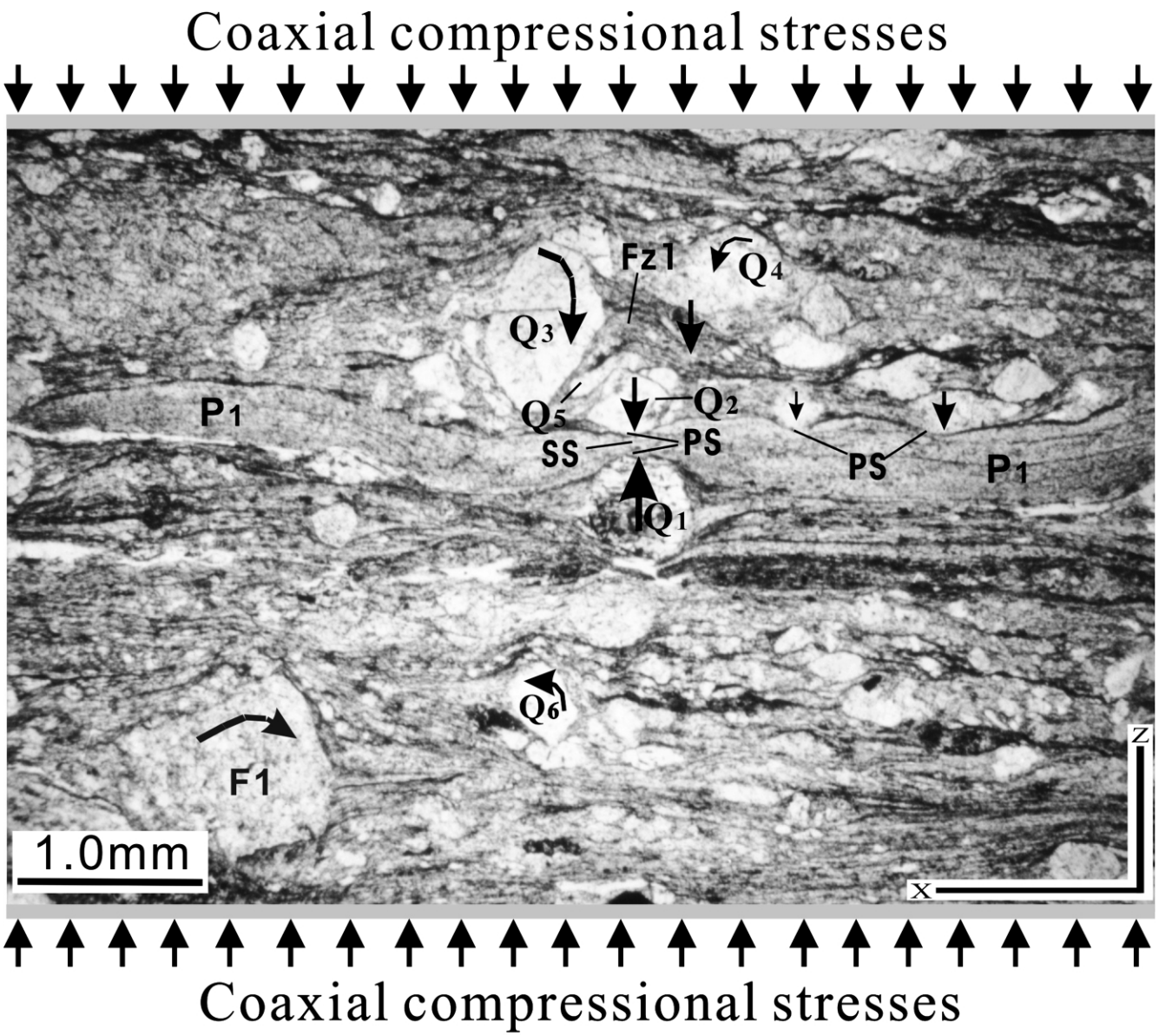

Fig. 10. Microphotographs of a deformed conglomerate (Sample p11-31) in *XZ*section from the Nanbeidagou area. Where a stretched pebble (P_1) was strongly compressed by two quartz grains (Q1 and Q2), the shortened structure (SS) and pitted structures (PS) formed. Clockwise and counterclockwise rotations of quartz and feldspar in the matrix, such as Q3, Q4, Q6 and F1, are present. A folded quartz grain (Q5) and a folded foliation subzone (Fz1) are present beneath two adjacent quartz grains (Q3 and Q4), which rotated in opposite directions. The arrows show formation stresses of the folded quartz. Sample locations are shown in Fig. 8.

5. Petrofabrics and their dynamic significance

Petrofabrics of quartz schist and calcite schist from 22 sites in the JDCZ were analyzed by optical axial measurement using a Fuers rotation platform, and by X-ray petrofabric analyses in the Laboratory of Geomechanics of the China Academy of Geological Sciences. Sample sites and their corresponding petrofabrics are illustrated in Fig. 12.

The preferred orientations of optic axes of calcite (samples p15-16, p15-7, p11-36, p12-21 and p20-3) are point maxima perpendicular to the local foliation plane (*S*), with an axial symmetry. These fabrics in calcite are similar to those produced by coaxial compression in laboratory experiments (Turner and Weiss, 1963).

Preferred orientations of optical axes of quartz from quartz schist at 17 sample sites (p6-2, p8-1, p11-31, p11-45, p14-14, p15-13, p15-18, p16-7, p16-19, p16-20, p16-21, p17-6, p17-7, p22-6, L3, L4 and L28) are variable, and show point maxima perpendicular to foliation or parallel to lineation, or small circle girdles. They correspond to axial and orthorhombic symmetry, respectively. Compared with the results of deformation experiments of quartz (Tullis et al., 1973; Price, 1985), these symmetric small circle girdles are most likely due to coaxial compression perpendicular to foliation. These point maxima may have

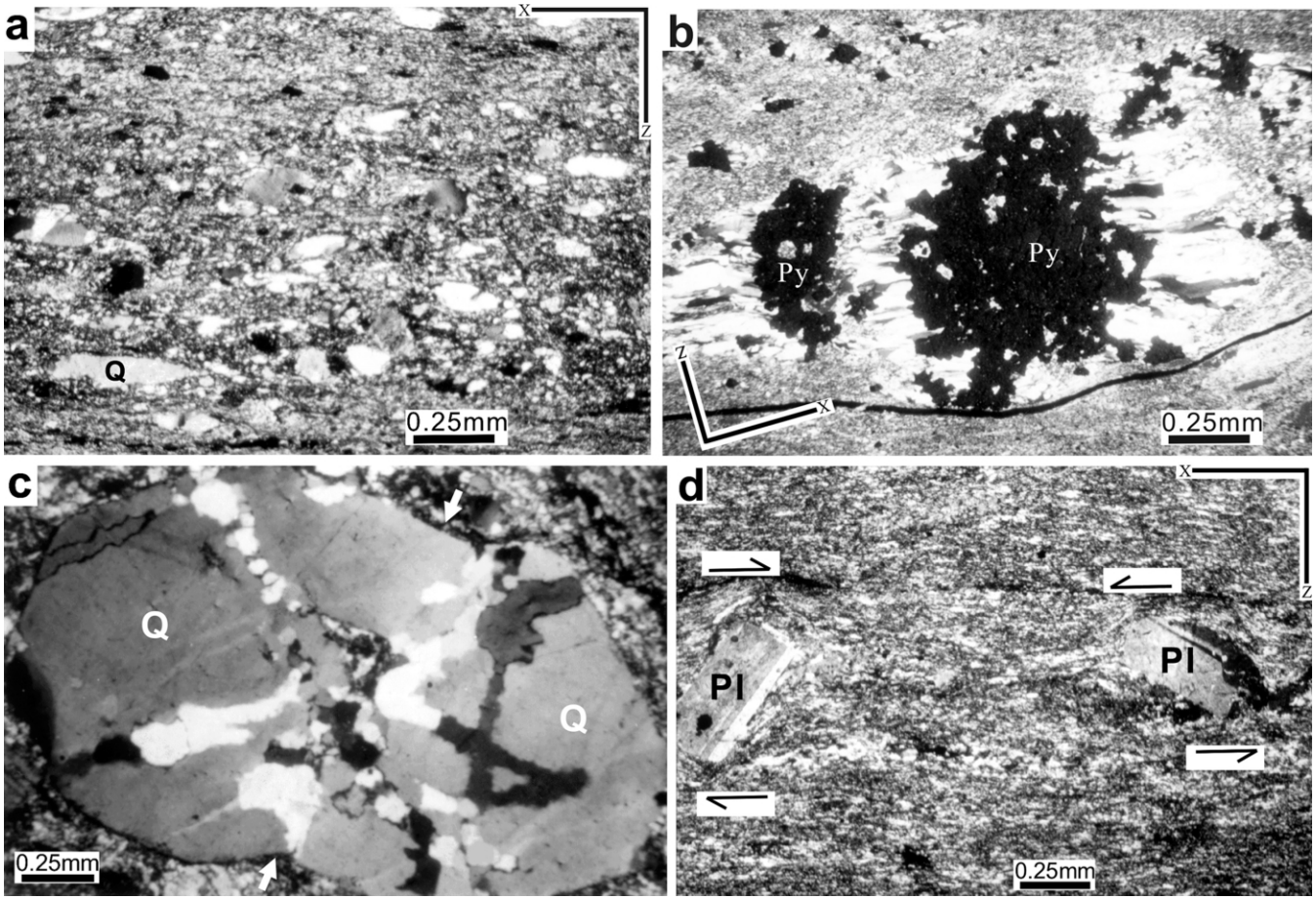

Fig. 11. Microphotographs of deformed clasts, pyroclastic and porphyroclastic structures. Sample locations are shown in Fig. 8. (a) Flattened quartz grains (Q) are parallel to the foliation that is defined by oriented sericite. Sample p16-21 from the Kanguer area. (b) Pressure shadows parallel to the foliation. Pyrite is black and quartz in pressure shadows is white. Sample p6-1 from the Kanguer area. (c) A set of conjugate intragranular fractures developed in a flattened quartz grain. The white arrows show the compressive direction. Sample p15-21 from the Nanbeidagou area. (d) A pair of porphyroclasts with opposite shear senses occurred in the same mylonitic zone. Sample p16-7 from the Kanguer area.

been produced by coaxial shortening (Lister and Hobbs, 1980; Price, 1985; Schmid and Casey, 1986; Zhong and Gua, 1991).

6. Strain analysis and strain pattern

6.1. Strain analysis

Strain markers, such as pebbles, quartz grains, ooids and pelitic nodules, were used to estimate the strain patterns of the JDCZ. The average initial axial ratio of pebbles and quartz grains in the JDCZ are measured and estimated as 2:1.5:1 and 1.5:1.25:1, respectively.

The strain of the JDCZ has been measured from 31 sites, including seven outcrops for coarse pebbles (CP) and coarse pelitic nodules (CPN), and 24 thin sections for fine pebbles (FP), fine pelitic nodules (FPN), quartz grains (QG) and ooids (O) (Table 1). Three principal axis lengths (x, y and z) of deformed coarse pebbles and pelitic nodules were measured directly in outcrops with more than 50 measurements for each site. Two thin sections (XZ section and YZ section) were made for every specimen, and almost all deformed markers in thin-section were outlined (Fig. 13) and their two principal axis lengths (x and z or y and z) measured. A total of more than 100 grains were measured in the two sections. Average ellipsoid shapes (Wheeler, 1986) of deformed markers were obtained by determining the geometric central point of the axis ratio plot area for outcrop data and the geometric average axis ratio of X/Z and Y/Z for thin-section data (Fig. 13), and used to calculate strain on the assumption of constant volume. The initial shape of pebbles and quartz grains were considered in the calculation. The strain data show that the Flinn k parameter varied significantly from 0.43 to 4.51, and the principal stretching strains change from 14 to 280% (Table 1).

6.2. Strain patterns and their distribution

There are three kinds of strain patterns in the JDCZ: apparent flattening, plane strain, and apparent constriction (Fig. 14), which are distributed regularly. Apparent

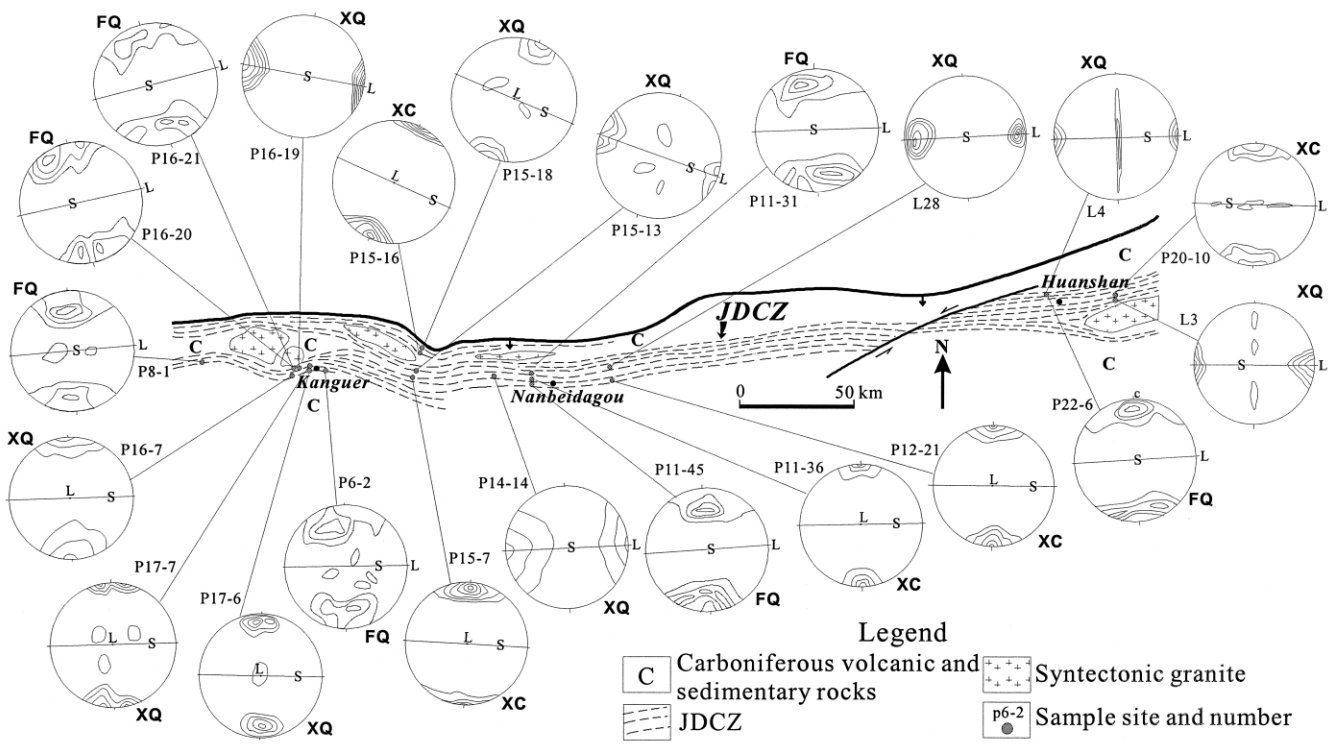

Fig. 12. Equal area and upper hemisphere projections of petrofabrics in the JDCZ. All the petrofabric projections are symmetrical to the foliation. FQ: *c*-axes of quartz with contours of 1–3–5–7%. XQ: *c*-axes of quartz with contours of 1–1.5–2.0–2.5–3.0%, determined by X-ray analysis. XC: *c*-axes of calcite with contours of 1–1.5–2.0–2.5–3.0%, determined by X-ray analysis.

flattening and plane strain predominate in the outer weekly deformed zones, while apparent constriction, especially with higher principal stretching strains ($e_1 > 1.00$), occurs mainly in the central zone of intensive deformation (Fig. 15). This suggests that the strain patterns are closely related to the deformation intensity. The strain patterns vary both longitudinally and laterally, and the strain is inhomogeneous.

6.3. Strain character

These strain patterns and attitudes of strain ellipsoids described above are referred to the local foliation and stretching lineation of the deformed rocks in the measured site. These are quite varied in the JDCZ and the overall strain pattern of the JDCZ is still unclear.

Tectonic coordinates, defined by the trend (E), the normal (S) and the downdip (D) of the entire EW-trending vertical foliation zone are used as a uniform reference frame in which to evaluate the strain character of the entire JDCZ. The relation between the tectonic coordinates (E, D and S) and attitude of the strain ellipsoid (*X*, *Y* and *Z*) is shown in Fig. 16. For convenience, the strain components of the principal strains parallel to the tectonic coordinates axes (E, D and S) are defined as the effective strain components with respect to the overall strain of the JDCZ, and called tectonic strain components (e_E, e_D and e_S) here. The tectonic strain components (e_E, e_D and e_S) of each site are calculated from principal strain (e_1, e_2 and e_3) as the following equations:

$$e_E = \frac{2mnl}{\sqrt{m^2n^2\sin^2\theta + l^2n^2\cos^2\theta\cos^2\alpha + m^2l^2\cos^2\theta\sin^2\alpha}} - 1 \quad (1)$$

$$e_D = \frac{2mnl}{\sqrt{m^2n^2\cos^2\beta + n^2l^2\sin^2\beta\sin^2(\alpha+\theta) + m^2l^2\sin^2\beta\cos^2(\alpha+\theta)}} - 1 \quad (2)$$

$$e_S = \frac{2mnl}{\sqrt{m^2n^2\sin^2\beta + n^2l^2\cos^2\beta\cos^2(\alpha+\theta) + m^2l^2\cos^2\beta\sin^2(\alpha+\theta)}} - 1 \quad (3)$$

where *m*, *n* and *l* represent three principal radii of the strain ellipsoid and are equal to $(1+e_1)/2$, $(1+e_2)/2$ and $(1+e_3)/2$, respectively, and α, β and θ represent the pitch angle of lineation (*X* axis) on foliation (*XY* plane), the dip angle of foliation and the angle between the strike of foliation in outcrop and that of the entire vertical foliation zone (eastern direction), respectively.

The results (Table 1) show that the N–S strain component (e_S) vary from −15 to −68%, with an average value of −36%. The average E–W stretching strain (e_E)

Table 1
Strain data from the JDCZ

Site	Measurement		Average ellipsoidal shape	Principal strain components						Attitude			Tectonic strain components		
	Marker	Number		e_1	e_2	e_3	Rxy	Ryz	K	α	β	θ	e_E	e_S	e_D
P8-5	QG	XZ-125/YZ-120	4.36:2.1:1	0.71	0	−0.41	1.73	1.68	1.03	0	85S	0	0.71	−0.41	−0.01
P7-5	CPN	91	7.56:4.2:1	1.39	0.33	−0.69	1.80	4.20	0.43	80E	80N	0	0.348	−0.68	0.44
P7-23	QG	XZ-123/YZ-118	2.64:1.25:1	0.46	−0.13	−0.17	1.68	1.05	1.60	25W	80S	0	0.27	−0.16	−0.08
P8-23	QG	XZ-116/YZ-122	2.53:1.26:1	0.41	−0.15	−0.16	1.67	1.01	1.66	5W	80N	10	0.36	−0.15	−0.13
P7-3	FP	XZ-75/YZ-54	6.34:2.39:1	0.85	−0.1	−0.42	1.99	1.59	1.25	85E	85N	10	−0.12	−0.42	0.77
P7-2	FP	XZ-69/YZ-59	4.36:2.76:1	0.37	0.16	−0.37	1.18	1.84	0.64	85E	85N	0	0.16	−0.37	0.35
P16-21	QG	XZ-132/YZ-120	4.75:1.57:1	1.00	−0.2	−0.37	2.52	1.26	2.01	15W	80SE	35	−0.03	−0.36	0.09
P18	CP	63	4.16:2.6:1	0.36	0.13	−0.35	1.20	1.73	0.69	70W	75SE	20	0.03	−0.33	0.23
P19	CP	55	4.5:2.5:1	0.45	0.07	−0.36	1.35	1.67	0.81	70W	75SE	20	−0.01	−0.34	0.28
P16-12	FP	XZ-67/YZ-68	3.86:1.9:1	0.43	−0.1	−0.26	1.52	1.27	1.20	60E	70N	15	−0.05	−0.24	0.21
P17-16	QP	XZ-132/YZ-120	2.8:1.5:1	0.43	−0.1	−0.24	1.56	1.20	1.30	30W	85S	15	0.16	−0.23	0.07
P17-15	QP	XZ-121/YZ-114	3.2:1.4:1	0.60	−0.2	−0.25	1.90	1.12	1.70	30E	85S	10	0.18	−0.25	−0.04
P17-4	FPN	XZ-103/YZ-105	1.47:1.44:1	0.14	0.12	−0.22	1.02	1.44	0.71	60W	75N	5	0.12	−0.21	0.10
P6-3	QP	XZ-127/YZ-120	2.62:1.40:1	0.40	−0.1	−0.2	1.56	1.12	1.39	75E	75N	5	−0.08	−0.19	0.29
P6-17	QP	XZ-118/YZ-117	3.1:1.4:1	0.56	−0.2	−0.24	1.85	1.12	1.65	50E	80S	10	−0.05	−0.24	0.17
P15-14	FP	XZ-72/YZ-62	4.33:3.2:1	0.3	0.28	−0.4	1.01	2.13	0.48	40E	70S	0	0.29	−0.37	0.08
P14-4	CP	78	4.48:2.8:1	0.39	0.16	−0.38	1.20	1.87	0.64	70W	75S	0	0.18	−0.36	0.21
P14-11	FPN	XZ-115/YZ-109	2.5:1.7:1	0.54	0.05	−0.38	1.47	1.70	0.87	35E	70S	10	0.25	−0.35	0.06
P11-14	FP	XZ-62/YZ-68	6.9:4.24:1	0.61	0.32	−0.53	1.22	2.83	0.43	75E	75S	0	0.33	−0.52	0.22
P11-17	CPN	62	11:2.2:1	2.80	−0.2	−0.65	5	2.20	2.27	80E	80S	0	−0.19	−0.65	0.66
P11-31	FP	XZ-76/YZ-68	21.60:4.82:1	2.58	−0.16	−0.69	4.24	2.75	1.54	35W	80N	0	0.39	−0.69	−0.11
P13-10	FPN	XZ-130/YZ-120	2.7:2.2:1	0.49	0.21	−0.448	1.23	2.20	0.56	10W	85N	5	0.45	−0.45	0.21
P22-4	FP	XZ-65/YZ-55	3.63:2.0:1	0.35	−0.01	−0.26	1.36	1.33	1.02	15W	85S	0	0.31	−0.26	0.01
P22-6	CP	89	13:1.8:1	2.28	−0.40	−0.50	5.42	1.20	4.51	15E	80S	0	1.55	−0.49	−0.01
P20-8	CP	58	3.36:1.6:1	0.38	−0.1	−0.18	1.57	1.07	1.48	75W	75S	0	−0.08	−0.17	0.26
P20-4	FP	XZ-62/YZ-80	9.1:2.1:1	1.45	−0.25	−0.46	3.25	1.40	2.32	80E	80S	10	−0.25	−0.46	0.94
P3-3	FP	XZ-68/YZ-57	7.2:2.0:1	1.13	−0.2	−0.41	2.70	1.33	2.03	10W	80NW	20	0.33	−0.40	−0.11
P3-5	FP	XZ-178/YZ-200	4.0:2.5:1	0.34	0.11	−0.33	1.20	1.67	0.72	25W	85NW	15	0.19	−0.33	0.18
P3-7	QP	XZ-120/YZ-116	2.7:1.3:1	0.46	−0.2	−0.19	1.73	1.04	1.66	65W	80S	10	−0.15	−0.19	0.32
P2-5	O	XZ-178/YZ-200	2.2:2.1:1	0.32	0.26	−0.4	1.05	2.10	0.50	0	70NE	15	0.18	−0.37	0.07
P1-12	CPN	67	5.7:1.5:1	1.79	−0.3	−0.51	3.80	1.50	2.53	0	85NW	15	0.58	−0.51	−0.28
The average values of tectonic strain from 31 sites													0.20	−0.36	0.18

and the average vertical stretching strain (e_D) are about 20 and 18%, respectively.

It is evident that the overall tectonic strain pattern, defined by the average values of the tectonic strain components from the 31 sites, is an apparent flattening, with a N–S shortening component and E–W and vertical extension. The total amount of shortening is more than 11 km and up to 27 km, with a shortening ratio of 36%. The amount of horizontal stretching is approximately 71 km with a stretching ratio of 20%, and the average vertical stretching ratio is 18%.

The relations among the distribution of principal strain patterns, foliation and lineations, and the overall tectonic strains indicate that the JDCZ has a 'cream-cake' strain character (Fig. 17; Ramsay and Huber, 1987). The mass flowed radially with apparent constriction in the middle intensive deformation zone. Plane strain and apparent flattening are distributed in the outer subzones. The 'cream-cake' strain character suggests that the JDCZ was formed by coaxial compression perpendicular to the JDCZ (e.g. Ramsay and Huber, 1987).

7. Dynamic metamorphism and PT conditions

The metamorphism in the JDCZ is characterized by progressive metamorphism. Fine-grained minerals (usually smaller than 10 μm), such as quartz and calcite, are recrystallized. However, dynamic recrystallization of larger (usually larger than 200 μm) mineral clasts, crystal fragments and phenocrysts of quartz and feldspar is common too. Some new metamorphic minerals, such as sericite, chlorite, chloritoid, biotite, muscovite, tremolite, diopside, and serpentine, were formed during the ductile deformation.

The greenschist metamorphic facies can be subdivided into chlorite–tremolite–phengite subfacies and chlorite–diopside–biotite subfacies. The chlorite–diopside–biotite subfacies is indicative of a relatively higher metamorphic temperature of 500–600 °C (Winkler, 1979) and is located in the middle deformation zone of the JDCZ, whereas the chlorite–tremolite–muscovite subfacies with a temperature of 400–500 °C (Winkler, 1979) is present in the southern and northern outer deformation zones. The si content of phengite in the JDCZ is about 3.2, suggesting a metamorphic pressure

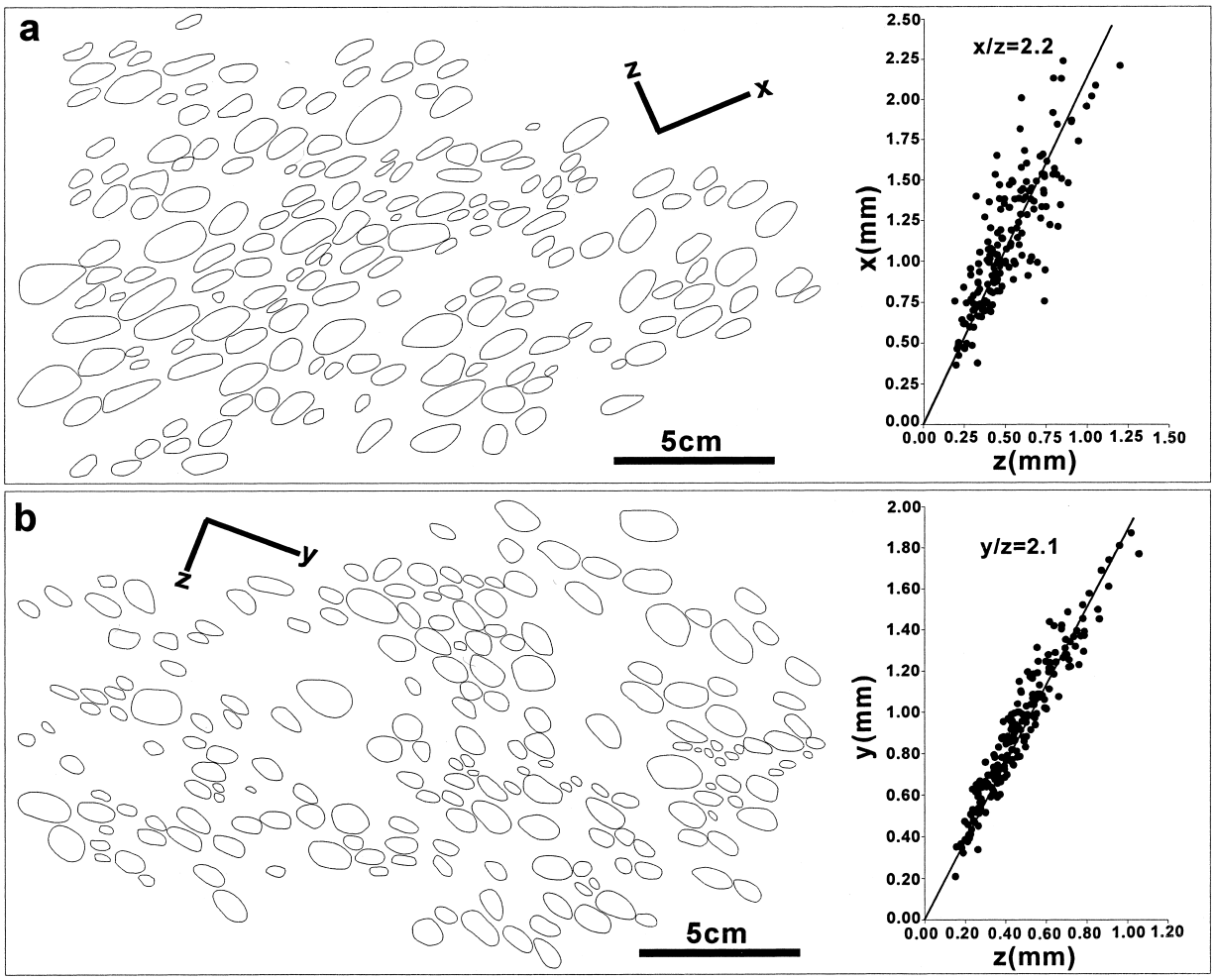

Fig. 13. Outlines of deformed ooids and plots of principal axis length in *XZ* section (a) and *YZ* section (b) of specimen p2-5 from the Huanshan area.

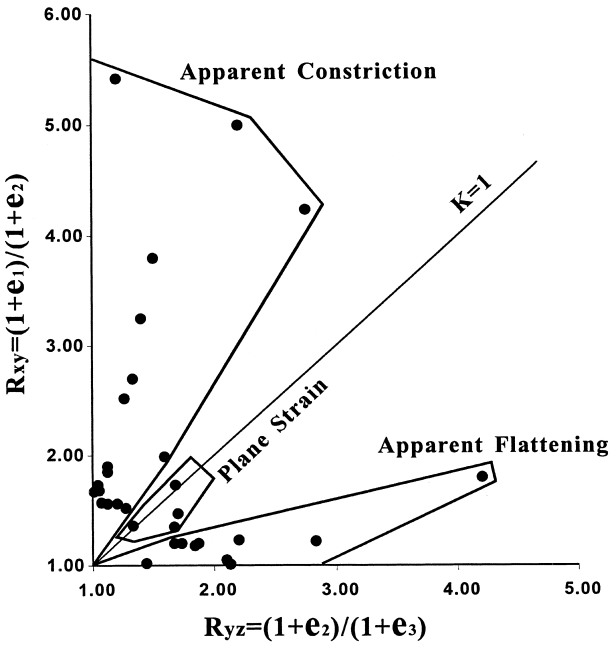

Fig. 14. Flinn plots of strain data from the JDCZ.

as high as 300–400 MPa (Velde, 1967), corresponding to a minimum depth of 10 km.

8. Dynamic origin and evolution of the JDCZ

8.1. Dynamic origin

The radial stretching lineations at large scale and bi-directional rotation of large grains at small- and micro-scale indicate that there is no uniform shear sense throughout the JDCZ, and simple shear deformation occurs only locally. The ‘cream-cake’ strain character of the JDCZ shows that the crust in the Jiaoluotage area was flattened during ductile deformation. The geometric and kinematic characteristics, including various typical contractional structures, and symmetric petrofabrics of deformed minerals, indicate that the JDCZ was formed from a N–S-oriented horizontal compression that was perpendicular to the JDCZ.

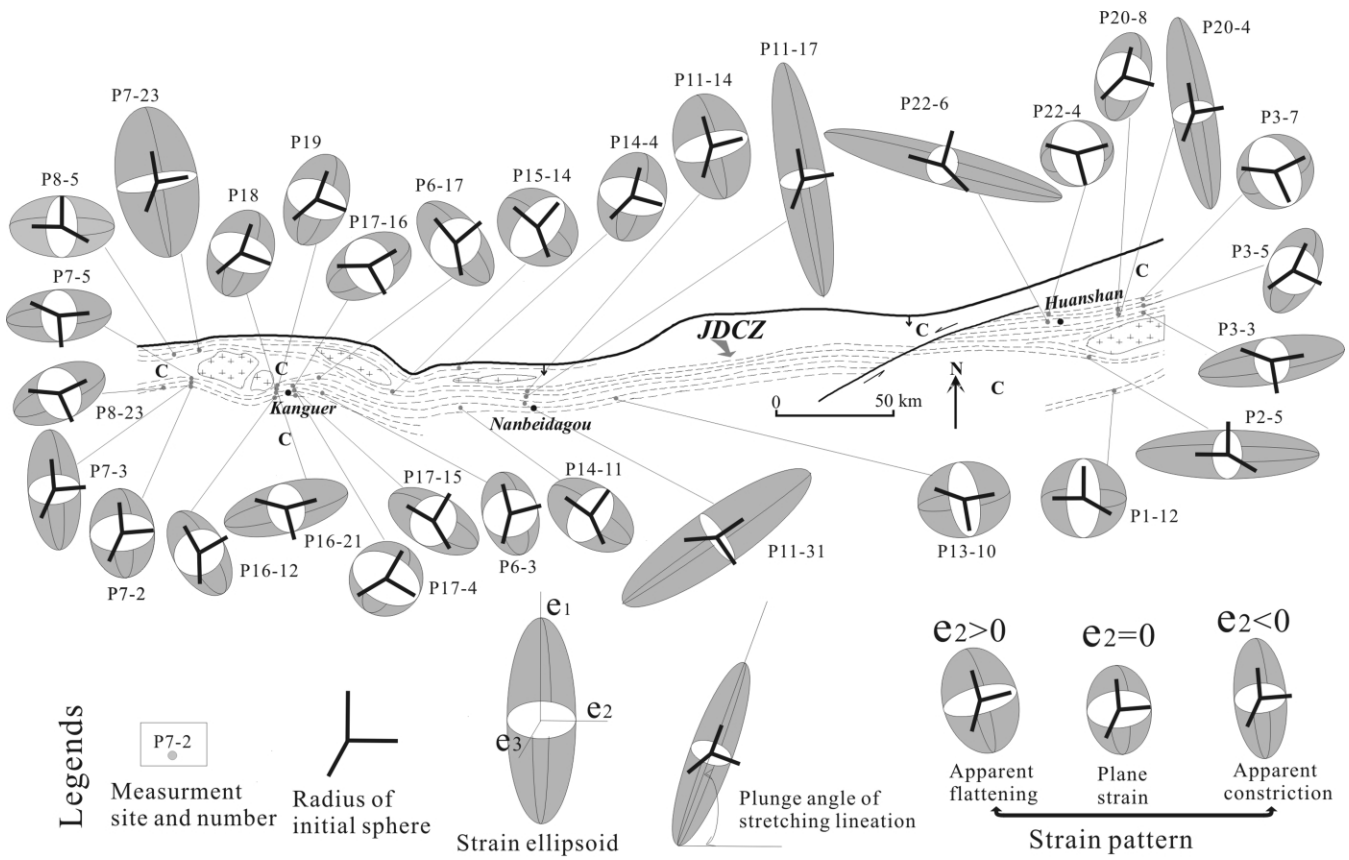

Fig. 15. A map showing the strain patterns of the JDCZ. Apparent flattening and plane strain predominate in the northern and southern outer zones of weak deformation, while apparent constriction, especially that with higher principal stretching strain ($e_1 > 1.00$), is mainly present in the middle intensive deformation zone.

8.2. Tectonic evolution of the JDCZ

The ages of dynamic metamorphism and syntectonic intrusive rocks (Ji et al., 1994; Yang et al., 1999) indicate that the JDCZ formed in the early Permian between 270 and 290 Ma. This is consistent with the closure time of the Tarim paleo-ocean (Hao and Liu, 1993) and the rapid expansion stage of the paleo-Tethyan ocean to the south (Pang, 2000). The coincidence in time suggests a genetic relation between the formation of the JDCZ and the other two tectonic events.

During the Carboniferous, the Tarim paleo-ocean plate was subducted beneath the Jungar plate, resulting in the separation of the middle Tianshan terrane from the Jungar

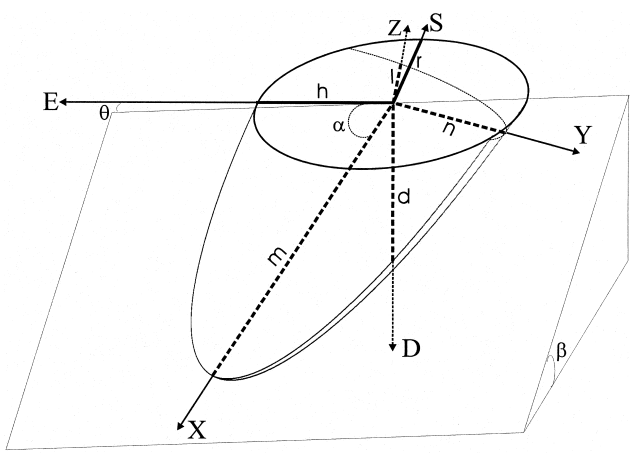

Fig. 16. A sketch of the relations between the tectonic coordinates (E, S, D) and the axes of the strain ellipsoid (*X, Y, Z*). The *m, n*and *l* are three principal stretches of the strain ellipsoid, and *h, r*and *d* are tectonic strain components in the tectonic coordinate axis direction. The α, β and θ are the pitch angles of the stretching lineation on the foliation, the dip angle of the foliation and the angle between the strike of the foliation and that of the entire vertical foliation zone (E–W direction), respectively.

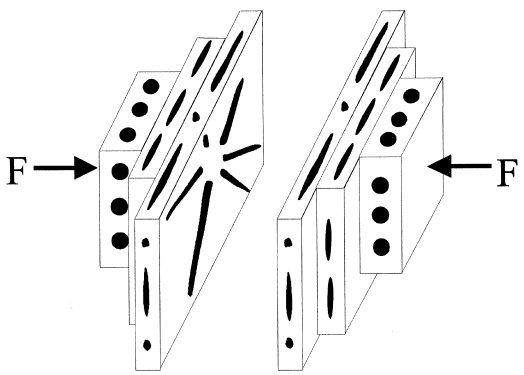

Fig. 17. Strain character and dynamic model of the JDCZ. Radial stretching lineations and intensive flattening effects indicate a typical 'cream-cake' strain character.

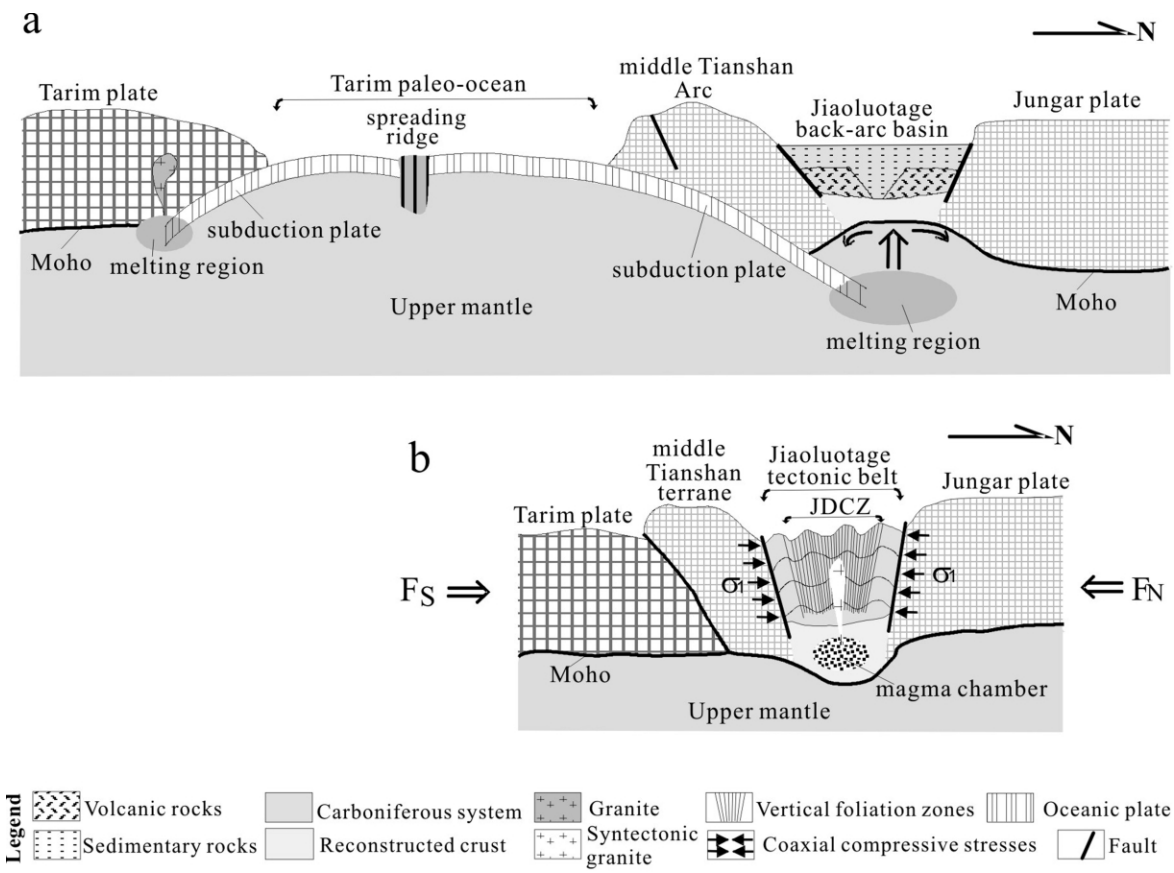

Fig. 18. Sketch of dynamic origin of the JDCZ. (a) During the Carboniferous, (b) during the Permian.

plate and the formation of the middle Tianshan arc and Jiaoluotage back-arc basin (Xiao and Feng, 1990; Ma et al., 1990, 1997; Sheng and Jin, 1993; Liu et al., 1995). In the early Permian, the paleo-Tethyan ocean was expanded rapidly (Pang, 2000), such that the Tarim paleo-ocean plate was driven northwards and collided with the middle Tianshan terrane. Sedimentary and volcanic rocks in the Jiaoluotage basin were intensively compressed. As a result, a macro-scale high-strain zone (JDCZ) was formed. The symmetric fabrics in the JDCZ were related to a coaxial horizontal compressive stress (Fig. 18).

9. Conclusion

The vertical JDCZ, composed of Carboniferous sedimentary and volcanic rocks, is characterized by augen structures in plan view and fan-like geometry in transverse profiles. It contains radial stretching lineations, and symmetric compressional structures and petrofabrics of deformed minerals, and has a 'cream-cake' strain character. The JDCZ was formed by N–S-oriented horizontal coaxial compression, caused by the collision between the Tarim paleo-ocean plate and the middle Tianshan arc–Jiaoluotage basin–Jungar plate system in the early Permian (270–290 Ma).

Acknowledgements

This study is supported by the MGMR of China (Grant zkd92-37), the National Natural Science Foundation of China (Grant numbers 49802021, 40272090 and 40072028) and CAS Knowledge Innovation Project (kzcx3-sw-137). We would like to express our gratitude to Dianqing Sun, Jiliang Li, Xuchang Xiao, Yadong Zheng, Yucheng Chai, and Xiaofeng Wang for valuable suggestions and discussions. The paper was significantly improved by the thorough and incisive reviews of Stephen G. Peters, SheFa Chen and an anonymous reviewer.

References

Bauer, R.L., Hudleston, P.J., 1995. Transpression-induced ductile shear in the boundary region of the Quetico and Wawa subprovinces, NE Minnesota—a response to local strain partitioning. In: Ojakangas, R.W., Dickas, A.B., Green, J.C. (Eds.), Basement Tectonics 10—Proceeding of the Tenth International Conference on Basement Tectonics, Kluwer Academic Publishers, London, pp. 367–377.

Bell, T.H., 1978. Progressive deformation and reorientation of fold axes in a ductile mylonite zone: the Woodroffe thrust. Tectonophysics 44, 285–320.

Choukroune, P., Gapais, D., 1983. Strain pattern in the Aar granite (Central Alps)—orthogneiss developed by bulk inhomogeneous flattening. Journal of Structural Geology 5, 411–418.

Clough, C.T., 1897. The geology of Cowal. Memoirs of the Geological Survey, Scotland, 8–11.

Fletcher, J.M., Bartley, J.M., 1994. Constrictional strain in a non-coaxial shear zone: implications for fold and rock fabric development, central Mojave metamorphic core complex, California. Journal of Structural Geology 16, 555–570.

Griggs, D.T., 1936. Deformation of rocks under high confining pressure. Journal of Geology 44, 541–577.

Griggs, D.T., 1940. Experimental flow of rocks under conditions favoring recrystallization. Bulletin of Geological Society of America 51, 1001–1022.

Hao, J., Liu, X., 1993. Ophiolite melange time and tectonic evolutional model in south Tianshan area. Scientia Geologica Sinica 28, 93–95. (in Chinese).

Holdsworth, R.E., 1990. Progressive deformation structures associated with ductile thrusts in the Moine Nappe, Sutherland, N. Scotland. Journal of Structural Geology 12, 443–452.

Hu, H., Wang, Z., Tu, G., 1997. Geological Evolution, Diagnoses and Mineralization in Northern Xinjiang, Science Publishing House, Beijing, pp. 1–234, (in Chinese).

Ji, J., Tao, H., Zeng, Z., Yang, X., 1994. Geology and Metallogeny of Kanggurtag Gold Mineralization Belt, Eastern Tianshan Mountains, Geological Publishing House, Beijing, pp. 1–190, (in Chinese with English abstract).

Lee, J.S., 1945. Theory and Technique of Geomechanics, Chongqing University Press, Chongqing, pp. 1–60.

Lee, J.S., 1946. A bended pebble. Sciences 157, 590.

Lister, G.S., Hobbs, B.E., 1980. The simulation of fabric development during plastic deformation and its application to quartzite, the influence of deformation history. Journal of structural Geology 2, 355–372.

Liu, D., Tan, Y., Zhou, R., 1995. The five stage evolution model of the Paleozoic crust in Xinjiang. In: Zhang, L.C. (Ed.), Bureau of Geology and Mineral Resources of Xinjiang. Proceeding in Geology and Mineral Resources in Tianshan Mountains, pp. 1–7 (in Chinese).

Ma, R., Ye, S., Wang, S., 1990. Evolution and tectonic framework of the eastern Tianshan Orogen. Geological Sciences in Xinjiang 2, 21–36. (in Chinese with English abstract).

Ma, R., Shu, L., Su, J., 1997. Tectonic Evolution and Metallogeny of Eastern Tianshan Mountains, Geological Publishing House, Beijing, pp. 1–11, (in Chinese with English abstract).

Pang, Y., 2000. Geological Evolution of the Karakorum–Kunlun Mountains, Science Publishing House, Beijing, pp. 509–525, (in Chinese).

Price, C.P., 1985. Preferred orientations in quartzites. In: Wenk, H.R., (Ed.), Preferred Orientations in Deformed Metals and Rocks, Academic Press, London, pp. 385–406.

Ramsay, J.G., 1980. Shear zone geometry: a review. Journal of Structural Geology 2, 83–99.

Ramsay, J.G., Graham, R.H., 1970. Strain variation in shear belts. Canadian Journal of Earth Sciences 7, 786–813.

Ramsay, J.G., Huber, M.I., 1987. The Techniques of Modern Structural Geology, Volume 2: Folds and Fractures, Academic Press, New York, pp. 308–700.

Sanderson, D.J., 1973. The development of fold axes oblique to the regional trend. Tectonophysics 16, 55–70.

Sanderson, D.J., Marchini, W.R.D., 1984. Transpression. Journal of Structural Geology 6, 449–458.

Schmid, S.M., Casey, M., 1986. Complete fabric analysis of some commonly observed quartz c-axis patterns. Geophysics Monograph 36, 263–286.

Sheng, Y., Jin, C., 1993. Magmatism and Gold Mineralization in Western Jungar, Science Publishing House, Beijing, pp. 1–23, (in Chinese).

Tullis, J.A., Christie, J.M., Griggs, D.T., 1973. Microstructures and preferred orientation of experimentally deformed quartzite. Bulletin of Geological Society of America 84, 297–314.

Turner, F.J., Weiss, L.E., 1963. Structural Analysis of Metamorphic Tectonites, McGraw-Hill Book Company, New York.

Velde, B., 1967. Si^{+4} content of natural phengites. Contributions to Mineralogy and Petrology 14, 250–258.

Wang, J., 1949. Review on the classification of cataclastic metamorphic rocks. Geological Review 14, 1–11.

Wheeler, J., 1986. Average properties of ellipsoidal fabric: implications for two-and three-dimensional methods of strain analysis. Tectonophysics 126, 259–270.

White, S.H., Burrows, S.E., Carreras, J., Shaw, N.D., Humphreys, F.J., 1980. On mylonites in ductile shear zones. Journal of Structural Geology 2, 175–188.

Williams, G.D., 1978. Rotation of contemporary folds into the X direction during overthrust processes in Laksefjord, Finnmark. Tectonophysics 48, 29–40.

Winkler, H.G.F., 1979. Petrogenesis of Metamorphic Rocks, 5th ed, Springer-Verlag, Berlin, pp. 73–139.

Xiao, X., Feng, Y., 1990. Geotectonic evolution of the Northern Xinjiang. Geological Sciences in Xinjiang 1, 47–68.

Yang, X., Cheng, H., Ji, J., Cheng, Q., Luo, G., 1999. Analysis of gold and copper ore-forming systems with collision orogeny of the eastern Tianshan. Geotectonica et Metallogenia 23, 315–322.

Yue, S., Ma, R., 1990. Deformation of Rocks in Experiments and Tectonic–Diagenesis–Mineralization. Changchun University Press, Jiling, 80–100.

Zheng, Y., Chang, Z., 1985. The Finite Strain Analysis and Ductile Shear Zone, Geological Publishing House, Beijing, pp. 1–150, (in Chinese).

Zheng, Y., Wang, Y., Liu, R., 1988. Sliding-thrusting tectonics caused by thermal uplift in the Yunmeng Mountains, Beijing, China. Journal of Structural Geology 2, 135–144.

Zhong, Z., Gua, B., 1991. Tectonite and Microstructure, Publishing House of China University of Geosciensecs, Wuhan, pp. 1–100, (in Chinese).